

12.5 Gbit/s carrier-injection-based silicon micro-ring silicon modulators

Qianfan Xu, Sasikanth Manipatruni, Brad Schmidt, Jagat Shakya, and Michal Lipson

School of Electrical and Computer Engineering
Cornell University, Ithaca, NY 14853
lipson@ece.cornell.edu

Abstract: We show a scheme for achieving high-speed operation for carrier-injection based silicon electro-optical modulator, which is optimized for small size and high modulation depth. The performance of the device is analyzed theoretically and a 12.5-Gbit/s modulation with high extinction ratio >9dB is demonstrated experimentally using a silicon micro-ring modulator.

©2007 Optical Society of America

OCIS codes: (130.3120) Integrated optics devices; (230.2090) Electro-optical devices; (250.5300) Photonic integrated circuits

References and Links

1. D. A. B. Miller, "Optical interconnects to silicon," *IEEE J. Sel. Top. Quantum Electron.* **6**, 1312–1317 (2000).
2. J. D. Meindl, J. A. Davis, P. Zarkesh-Ha, C. S. Patel, K. P. Martin, and P. A. Kohl, "Interconnect opportunities for gigascale integration," *IBM Res. Dev.* **46**, 245–263 (2002).
3. R. A. Soref, and B. R. Bennett, "Electrooptical effects in silicon," *IEEE J. Quantum Electron.* **23**, 123-129 (1987).
4. A. Liu, R. Jones, L. Liao, D. Samara-Rubio, D. Rubin, O. Cohen, R. Nicolaescu, and M. Paniccia, "A high-speed silicon optical modulator based on a metal-oxide-semiconductor capacitor," *Nature* **427**, 615-618 (2004).
5. Q. Xu, B. Schmidt, S. Pradhan, and M. Lipson, "Micrometre-scale silicon electro-optic modulator," *Nature* **435**, 325-327 (2005).
6. G. Gunn, "CMOS photonics™ - SOI learns a new trick," in *Proceedings of IEEE International SOI Conference* (Institute of Electrical and Electronics Engineers, New York, 2005), pp. 7-13.
7. T. Sadagopan, S. J. Choi, S. J. Choi, P. D. Dapkus, and A. E. Bond, "Optical modulators based on depletion width," *IEEE Photon. Technol. Lett.* **17**, 567-569 (2005).
8. J. Niehusmann, A. Vörckel, P. H. Bolivar, T. Wahlbrink and W. Henschel, "Ultrahigh-quality-factor silicon-on-insulator microring resonator," *Opt. Lett.* **29**, 2861-2863 (2006).
9. R. F. Pierret, *Semiconductor Device Fundamentals* (Addison Wesley, 1996), Chap 8.
10. Q. Xu, B. Schmidt, J. Shakya, and M. Lipson, "Cascaded silicon micro-ring modulators for WDM optical interconnection," *Opt. Express* **14**, 9431-9435 (2006).

1. Introduction

A silicon electro-optical modulator is a critical component for enabling optical interconnection systems on a microelectronic chip [1, 2]. Several silicon modulators based on the free-carrier dispersion effect [3] in silicon have been demonstrated experimentally [4-6]. These modulators are either based on metal-oxide-semiconductor (MOS) capacitors [4] or p-i-n diodes [5, 6]. The p-i-n diodes can either work with high carrier injection using forward bias voltage above the diode threshold voltage [5], or be confined to voltage below threshold and rely on the depletion width modulation.

The carrier-injection-based p-i-n modulator, in contrast to the other silicon-base modulators, can provide large changes of refraction index and high modulation depths in micron-size devices. However, it is conventionally thought to be a slow device. The higher modulation depth comes from the fact that it does not suffer from either small optical confinement factor (in the case of the MOS capacitor [4]) or low carrier density in the active

region (in the case of the depletion-based p-i-n diode [6, 7]), while its speed is limited since it relies on the slower diffusion of minority carriers, as opposed to the faster motion of majority carriers. Here we show both theoretically and experimentally, a driving scheme for greatly enhancing the operation speed of the carrier-injection based p-i-n modulator. Using this method and the micro-ring resonator structure, we achieve simultaneously high-speed operation above 10 Gbit/s, small device size, low power consumption and high modulation depth.

2. Device parameters and dc performances

The structure of the device used in the experiment is shown in the inset of Fig. 1. It consists of a ring resonator with the radius of 5 μm , with a p-i-n junction embedded in, side-coupled to a waveguide. The waveguide and the ring are formed by silicon strips with the height of 200 nm and the width of 450 nm on top of a 50-nm-thick slab layer. The distance between the ring and the straight waveguide is ~ 200 nm. The fabrication process is similar to that presented in Ref. [5]. The main differences between the device structure shown here and that present in Ref. [5] is that an additional n^+ -doped region is added outside of the straight waveguide to form nearly closed p-i-n junctions, and the distance between the doped regions and the edge of the ring resonators and straight waveguides is reduced to ~ 300 nm from ~ 1 μm in Ref. [5]. Note that this device is fabricated using the e-beam lithography, however similar devices have been fabricated using the deep-UV lithography in CMOS fabrication facilities [6], indicating a complete CMOS compatibility.

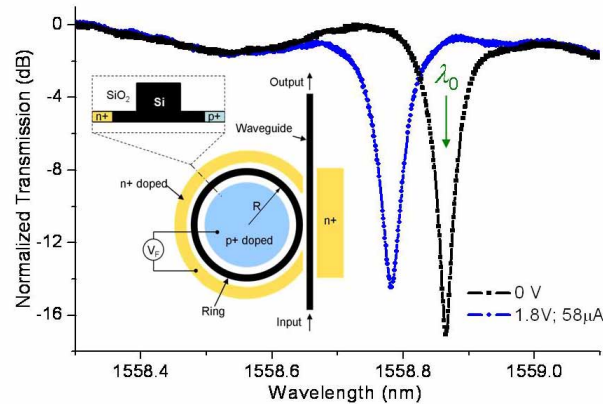


Fig. 1. Normalized transmission spectra of the modulator. Black line: transmission spectrum with 0V applied on the p-i-n junction. Blue line: transmission spectrum with 1.8V on the junction. The dc current at this voltage is 58 μA . Inset: schematic of the device structure.

The transmission spectrum of the quasi-TE mode of the modulator is measured with a tunable laser. The black line in Fig. 1 shows the normalized transmission spectrum when the bias voltage on the device is 0V. At the resonant wavelength λ_0 of the ring resonator, light is coupled into the ring resonator and lost due to the scattering from the side-wall roughness of the ring, causing a spectral dip at this wavelength. The quality factor of the ring resonator is $Q \approx 20,000$. All the analyses and experiments hereafter assume the wavelength of the input light is fixed at the 0-V resonant wavelength λ_0 . When the bias voltage on the device is increased to 1.8V and the dc current is measured to be 58 μA , the resonance of the ring resonator blue-shifts due to the accumulation of free carriers in the ring and the corresponding decrease of the refractive index of the silicon [3-5]. One can clearly see that the transmission of light at λ_0 increases significantly. Therefore, the output optical power can be modulated by applying different voltages on the device. Note that due to the limited precision of the fabrication process, the resonant wavelength of the ring resonator varies in a range of ~ 1 nm. This variation can be compensated by a local temperature change of ~ 10 $^\circ\text{C}$. The critical coupling

condition, which determines the depth of the resonance, is much more tolerant to fabrication variations and temperature shifts. Experiments show that more than 50-nm variation of the distance between the ring and the waveguide can be tolerated while maintaining > 10dB extinction ratio.

3. Enhancing the modulation speed

The operation speed of the p-i-n modulator is conventionally thought to be limited by the relatively slow carrier dynamics in the junction. However, the optical response time, in contrast to the electrical response time, can be much shorter thanks to the nonlinear transfer function of the device, enabling much faster modulation.

The nonlinear relationship between the optical transmission T at the wavelength λ_0 and the total charge Q in the junction is given by:

$$T = 1 - \frac{1}{1 + (Q/Q_0)^2} \quad (1),$$

where

$$Q_0 = \frac{qn_g \cdot \mathbb{V}}{\Gamma n_f \cdot 2Q} \approx 2.2 \times 10^{-14} \text{ C} \quad (2);$$

$q = 1.6 \times 10^{-19} \text{ C}$ is the electron charge; $n_g = 4.3$ is the group index of the ring; $\mathbb{V} = 4.5 \times 10^{-12} \text{ cm}^3$ is the volume of the junction; $\Gamma = 0.8$ is the mode confinement factor; $n_f \approx 4.3 \times 10^{-21} \text{ cm}^3$ is the ratio between the change of refractive index of silicon and the electron-hole-pair density ΔN when $\Delta N \sim 10^{17} \text{ cm}^{-3}$ [3]; and $Q \approx 20,000$ is the quality factor of the ring resonator. For simplicity, we assume that the ring resonator is critically coupled to the waveguide [8], so that the optical transmission is zero at λ_0 . When the p-i-n diode is forward biased, the electron and hole densities in the intrinsic region are equal, which means that the total charge carried by electrons and holes satisfies $Q_h = -Q_e = Q$. Under dynamic driving voltage, the charge Q in the junction follows the following differential equation [9]:

$$\frac{dQ(t)}{dt} = i(t) - \frac{Q(t)}{\tau_c} = \frac{v(t) - v_j(t)}{R} - \frac{Q(t)}{\tau_c} \quad (3),$$

where v is the externally applied voltage; v_j is the voltage drop on the junction; R is the serial resistant of the diode, determined mostly by the contact resistant at the metal-silicon interface; and τ_c is the average carrier recombination lifetime in the device.

The rise time of the optical transmission is much shorter than the rise time of the charge dynamics, which is determined by the carrier dynamics with positive bias voltage $+V_1$:

$$\frac{dQ(t)}{dt} = \frac{V_1 - v_{th}}{R} - \frac{Q(t)}{\tau_c} \quad (4),$$

where $v_{th} \approx 0.7 \text{ Volt}$, close to the threshold conditions. The steady-state value of the charge is $Q_s = (V_1 - v_{th}) \tau_c / R$. The rise time of the charge injection, defined as the time needed for Q to reach $0.9Q_s$ is $2.3 \tau_c$, which is $\sim 1 \text{ ns}$ in the modulator used in the experiment. On the other hand. From Eq. (1) one can see that the optical transmission quickly saturates to $\sim 100\%$ as the charge Q increases. Specifically, the transmission $T > 90\%$ as long as the charge $Q > 3Q_0$. Therefore, the optical rise time t_r is only determined by the time needed to inject $\sim 3Q_0$ into the junction, which can be much shorter than the rise time of charge injection, if $3Q_0$ is much smaller than Q_s . In Fig. 2(a) we plot an ideal NRZ signal between $+V_1$ and $-V_2$ at 5 Gbit/s, where $+V_1$ represents logic '1' and $-V_2$ represents logic '0'. When the device is driven by this signal, the carrier dynamics of the modulator and optical transmission are simulated based on Eq. (3) and Eq. (1), and shown in Fig. 2(b) and Fig. 2(c). By comparing the rising edge of Fig. 2(b) and Fig. 2(c). One can clearly see that the optical rise time t_r is much shorter than the electrical rise time determined by τ_c . The optical rise time can be further decreased by using a higher V_1 . Higher V_1 , however, leads to higher steady-state charge Q_s , which in turn increases

the time for the carriers to be fully extracted from the junction with reverse bias, as we will show next.

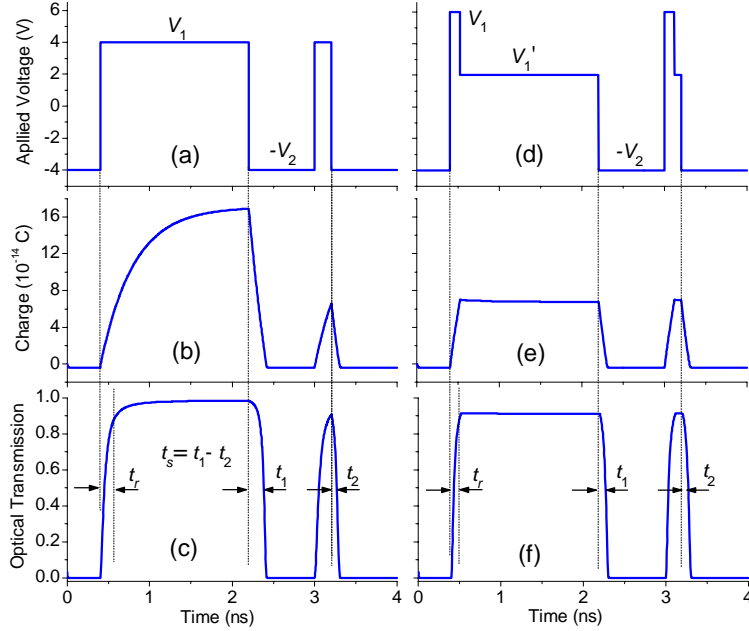


Fig. 2. Calculated dynamics of the micro-ring modulator. (a): NRZ driving signal at 5 Gbit/s; $V_1 = V_2 = 4\text{V}$. (b): Total charge in the junction with driving voltage of (a). (c): Optical transmission of the ring resonator; $t_r = 192\text{ ps}$; $t_s = t_1 - t_2 = 114\text{ ps}$. (d): Pre-emphasized NRZ signal at 5Gbit/s; $V_1 = 6\text{V}$; $V_1' = 2\text{V}$; $V_2 = 4\text{V}$. (e): Total charge in the junction with driving voltage of (d). (f): Optical transmission of the ring resonator; $t_r = 110\text{ ps}$; $t_s = t_1 - t_2 \approx 0\text{ ps}$. In all the calculations, we used the experimentally measured serial resistance $R = 7.7\text{ k}\Omega$.

The fall time of the modulator is limited by the extraction time of the carrier. When the applied voltage on the device is switched to negative ($v = -V_2$), the carriers are extracted out of the junction through drifting. This process can be very fast since the time for electrons to drift across the μm -width junction can be as small as 10 ps. Given the finite serial resistance R , however, the total drift current is limited by V_2/R , which limits the time to fully extract the excessive carriers in the junction. Immediately after the applied voltage changes from positive to negative, the charge in the junction is still positive, therefore the junction voltage v_j remains to be close to v_{th} . After the charges stored in the junction are removed, the junction voltage v_j is determined by the depletion charge and the depletion-layer capacitance C_j . The charge dynamic follows

$$\frac{dQ(t)}{dt} = \frac{-V_2 - v_{th}}{R} - \frac{Q(t)}{\tau_c} \quad Q > 0 \quad (5);$$

$$\frac{dQ(t)}{dt} = \frac{-V_2 - Q(t)/C_j}{R} - \frac{Q(t)}{\tau_c} \quad Q \leq 0 \quad (6).$$

When it reaches steady state, the charge in the junction will be negative, representing the expansion of the depletion region. The depletion-layer capacitance C_j of the fabricated device is estimated from the junction parameters to be $\sim 1\text{fF}$. From the charge dynamics shown in Fig. 2(b), where $-V_2 = -4\text{V}$ is assumed, one can see the falling edge is indeed much sharper than the rising edge. However, as Eq. (1) shows, the optical transmission remains almost constant ($T > 90\%$) until the charge Q drops below $\sim 3Q_0$. Only after then does the optical transmission start to drop. This extra delay, which is called the charge storage time t_s , is proportional to the excess charge injected into the cavity ($Q_s - 3Q_0$). In order for the device to support a bit rate B , it's required that $t_s < 1/2B$. The increase of the charge storage time t_s , with

the increase of steady-state charges limits the forward-bias voltage than can be applied to the device, which in turn limits the optical rise time t_r . In Fig. 2(c), one can see that the optical transmission barely reached 90% in a single bit of '1', meaning $t_r \approx 1/B$, when $B = 5$ Gbit/s. On the other hand, the charge storage time t_s is slightly higher than $1/2B$, showing the device can hardly support the bit-rate of 5 Gbit/s with the given driving voltage. Apparently, we can not decrease the forward bias voltage V_1 to reduce t_s , because that increases t_r and makes $t_r > 1/B$.

In order to increase the modulation speed of this device, one need to break the tradeoff between the optical rise time and the charge storage time (t_r and t_s). We noticed that t_r only depends on the forward bias voltage V_1 before Q reaches the threshold value of $\sim 3Q_0$. After that, in order to avoid inject excess carriers into the junction, we can then reduce the bias voltage to V_1' , as shown in Fig. 2(d). With this approach the steady-state charge Q_s and the charge storage time t_s are determined by V_1' , while the rise time t_r is determined by V_1 . By using a high V_1 and a low V_1' , both the optical rise time t_r and the charge storage time t_s can be reduced, allowing for higher operation speed.

The effect of the pre-emphasized driving signal on the dynamics of the modulator can be seen in Fig. 2(e) and Fig 2(f), where we show the charge dynamics and the optical transmission when $V_1 = 6V$ and $V_1' = 2V$. The optical rise time t_r is measured to be 110ps while t_s is negligible. Therefore the bit-rate of 9 Gbit/s is supported. The bit-rate can be further increased with a higher V_1 . It's important to note that the pre-emphasis can also reduce the power consumption of the device by eliminating the injection of excess carriers and reducing the dc current through the device. With the pre-emphasis, the power consumption is mostly determined by the power needed to swing the necessary amount of charge ($\sim 3Q_0$) in and out of the p-i-n junction during each bit-flip. The reduced power consumption is also beneficial for the stability of the device, because of less heat generation.

4. Experimental demonstration of high-speed modulation

We verify experimentally the effect of pre-emphasis on the speed of the modulator. Figure 3 shows the experimental setup for generating the pre-emphasized NRZ signal. A NRZ signal from a pattern generator was amplified by a 12-Gbit/s inverting amplifier and sent to an impulse generator network (IGN), which acts as a differentiator, and output an impulse at each transition of the input NRZ signal. Then, these pulses are combined with the original NRZ signal, and amplified by a 20-GHz RF amplifier, creating the pre-emphasized NRZ signal, as illustrated by the red lines in the figure.

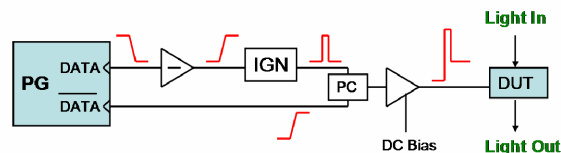


Fig. 3. Schematics of the experimental setup showing the generation of the NRZ driving signal with pre-emphasis. PG: pattern generator. IGN: impulse generator network. PC: power combiner. DUT: device under test.

The effect of the pre-emphasis is first examined using a low-repetition-rate square-wave signal. This signal is generated by repeating a fixed pattern of 16 consecutive '1's and 16368 consecutive '0's at the bit-rate of 12.5 Gbit/s. The blue and green lines in Fig. 4(a) show the NRZ driving signals when the IGN is disconnected. The blue and green lines in Fig. 4(b) show the waveform of the modulated optical output power obtained with a 30-GHz detector. When a low forward-biasing voltage of 2V is used (the blue lines), the optical rise time is very long. When a low forward-biasing voltage of 4V is used (the green lines), the optical rise time is greatly reduced, but a long charge storage time t_s appears due to the injection of excess carriers. By adding the pre-emphasis at the transition edges (the red lines), the output optical signal has both short rise time and short charge-storage time, allowing for high-bit-rate

operation. Note that the impulse generator also generates negative pulses at high voltage to low voltage transitions. Therefore the output signal after the combiner has pre-emphasis at both positive and negative transitions, as seen in Fig. 4(a). This is in contrast to Fig. 2(d), where only the pre-emphasis at positive transitions is assumed. The pre-emphasis at the negative transitions also helps to extract carrier faster, but is not essential to the high-speed operation.

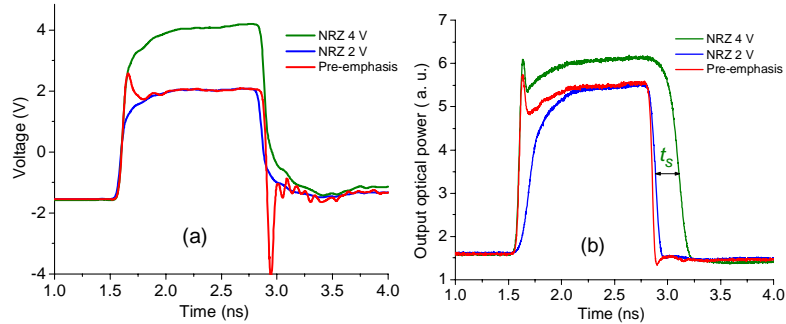


Fig. 4. (a). square-wave driving signals with (red line) and without (blue and green lines) the pre-emphasis. (b): the output optical power when the modulator is driven by voltage signals shown in (a).

In order to show the device operation at high bit-rates, we use a driving signal composed of a pseudo-random bit sequence (PRBS $2^{10}-1$) at 12.5 Gbit/s. The waveform and eye-diagrams are shown in Fig. 5. This signal composed of a NRZ signal with $V_{pp} \sim 8V$ and pre-emphasis pulses with height $\sim 4V$ at each transition edges. The eye-diagram of the output optical signal is shown in Fig. 6. One can see that the eye is completely open. The extinction ration of the modulated signal is ~ 9 dB. Note that the relatively high driving voltage used in the experiment can be greatly reduced when the contact resistance is reduced from that of the current device (7.7 k Ω). The pattern generator used in the experiment has slightly uneven bit widths for the even and odd bits, which results in the different widths between the two eyes in both electrical [Fig. 5(b)] and optical (Fig. 6) eye-diagrams. On the eye-diagram of the optical output (Fig. 6), one can see an overshoot on each rising edge of the signal. This behavior though appears similar to the pre-emphasis added on the driving signal, is not the result of the pre-emphasis. This behavior originates from the optical energy stored in the resonance mode of the ring resonator in the low-transmission mode. The stored energy is released into the output waveguide when the ring resonance is quickly detuned from the input wavelength, with tuning time comparable to the photon lifetime of the resonator. This phenomenon has been analyzed in detail in Ref. [10].

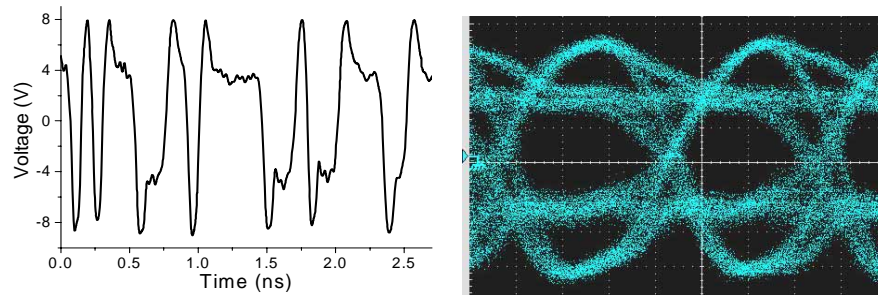


Fig. 5. The waveform and eye-diagram of the electrical driving signal with pre-emphasis at 12.5 Gbit/s.

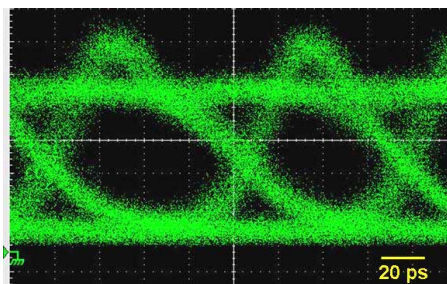


Fig. 6. Eye-diagrams of the modulated optical output at 12.5 Gbit/s with PRBS $2^{10}-1$.

5. Conclusion

In conclusion, we demonstrate 12.5 Gbit/s modulation with high extinction ratio using a silicon micro-ring modulator. The control of the dynamics of the modulator is achieved by engineering the NRZ driving signal. This work shows that simultaneous small device size, high modulation depth and high speed can be achieved in carrier injection devices.

Acknowledgments

This work was sponsored by the Defense Advanced Research Projects Agency's supervised by Dr. Jagdeep Shah. The program is executed by the ARO under Contract No. W911NF-06-1-0057 managed by Dr. Wayne Chang.